PHYSICAL REVIEW A **94**, 050101(R) (2016)

High sensitivity to variation in the proton-to-electron mass ratio in O_2^+

D. Hanneke,* R. A. Carollo, and D. A. Lane
Physics & Astronomy Department, Amherst College, Amherst, Massachusetts 01002, USA
(Received 25 July 2016; published 9 November 2016)

Molecular vibrational transitions are prime candidates for model-independent searches for variation of the proton-to-electron mass ratio. Searches for present-day variation achieve the highest sensitivity with deep molecular potentials. We identify several high-sensitivity transitions in the deeply bound O_2^+ molecular ion. These transitions are electric-dipole forbidden and have narrow linewidths. The most sensitive transitions take advantage of an accidental degeneracy between vibrational states in different electronic potentials. We suggest experimentally feasible routes to a measurement with uncertainty below current limits on present-day variation in m_p/m_e.

DOI: 10.1103/PhysRevA.94.050101

The dimensionless fundamental constants are the input parameters to our physical theories. Apparent variations of these constants arise naturally in many extensions to the standard model, including the spacetime evolution of additional dimensions or new scalar fields [1]. Recent work suggests that certain dark matter fields could induce oscillations in the values of fundamental constants [2].

The proton-to-electron mass ratio $\mu = m_p/m_e$ is particularly interesting because the two masses arise from different mechanisms. Variation would imply a change in the relative strengths of the strong and electroweak interactions. Models typically predict the relative change of μ should be of order 40 times larger than that of the fine-structure constant α [1].

Searches for variation of μ have been approached over both cosmological and laboratory time scales. The current precision of cosmological searches are at the level of $10^{-6} - 10^{-7}$ over $\sim 10^{10}$ yr [3–5]. The tightest bounds on present-day variation of μ come from atomic clock experiments, which set the limit $\dot{\mu}/\mu \lesssim 10^{-16}$ yr^{-1} [6,7]. In these experiments, nearly all the sensitivity to μ variation comes from the hyperfine structure of cesium, and extracting the precise μ dependence requires a model of the cesium nuclear magnetic moment [8].

The vibration and rotation of molecules provide a model-independent means to search for variation in μ [9–14]. The most stringent constraint from a molecular measurement is $\dot{\mu}/\mu = (-3.8 \pm 5.6) \times 10^{-14}$ yr^{-1} in SF_6 [15]. We propose O_2^+ as a molecule possessing a high sensitivity to present-day variation in μ as well as experimentally feasible means for measuring it. We describe two possible measurements, each of which is capable of resolving fractional changes in μ to better than 10^{-16} in 1 day with a single molecule. As discussed below, the high sensitivity arises from the molecule's deep electronic ground-state potential (54 600 cm^{-1}). Other molecules with deep potentials may also have suitable transitions.

Features of the relatively simple molecular structure of O_2^+ make it amenable for experiments. It is homonuclear, so nuclear symmetry eliminates half the rotational states and forbids electric dipole ($E1$) transitions within an electronic state. A homonuclear molecule's nonpolarity also suppresses many systematic effects [16–19], including some ac Stark and blackbody radiation shifts. The most common isotope of oxygen (^{16}O, 99.8% abundance) has no nuclear spin, so $^{16}O_2^+$ lacks a hyperfine structure. Unlike many molecular ions, O_2^+ has measured spectroscopic parameters [20–28] and existing theoretical calculations [29–33]. This prior work has been motivated in part because of the important role O_2^+ plays in the ionospheres of Earth and other planets [34]. Most relevant to the present work, several vibrational states in the middle of the O_2^+ ground $X\,^2\Pi_g$ potential are nearly degenerate with low vibrational states of the excited $a\,^4\Pi_u$ potential. This degeneracy should allow searches for variation in μ with high sensitivity in both the absolute and relative senses [35].

Searches for fractional changes in μ usually involve monitoring the energy difference $\hbar\omega$ between two energies with different μ dependence, $\hbar\omega = E'(\mu) - E''(\mu)$. The change in μ is then given by

$$\frac{\Delta\mu}{\mu} = \frac{1}{\mu}\left(\frac{\partial\omega}{\partial\mu}\right)^{-1}\Delta\omega = \left(\frac{\partial\omega}{\partial(\ln\mu)}\right)^{-1}\Delta\omega. \tag{1}$$

The absolute sensitivity of the transition is given by $\partial\omega/\partial(\ln\mu)$, which is sometimes called the absolute enhancement factor. In an experiment, the statistical precision with which $\Delta\omega$ can be measured is given by

$$\delta\omega = \frac{\Gamma}{\sqrt{M}\,S/\delta S}, \tag{2}$$

where Γ is the transition linewidth, $S/\delta S$ is the signal-to-noise ratio, and M the number of independent measurements (assuming white noise). Here, $\delta\omega$ represents the uncertainty in determining the change $\Delta\omega$. The figure of merit is thus

$$\frac{\partial\omega}{\partial(\ln\mu)}\frac{1}{\Gamma}. \tag{3}$$

In some cases, such as the Doppler-broadened lines encountered in astrophysical measurements, the linewidth is proportional to the transition frequency and the figure of merit is proportional to the relative enhancement factor $[\partial\omega/\partial(\ln\mu)]/\omega$. In other cases, such as O_2^+, such relative enhancement can be experimentally convenient.

Because of its importance in isotope shifts, the scaling of molecular parameters with μ has been known for some time

*dhanneke@amherst.edu

(see Sec. III.2.g in Ref. [36]). In particular, for a state of energy

$$E/(hc) = T_e + \omega_e\left(v+\tfrac{1}{2}\right) - \omega_e x_e\left(v+\tfrac{1}{2}\right)^2 + B_e J(J+1), \tag{4}$$

the electronic energy T_e is independent of μ, the vibrational coefficient ω_e scales as $\mu^{-1/2}$, the lowest anharmonicity coefficient $\omega_e x_e$ scales as μ^{-1}, and the rotational constant B_e scales as μ^{-1}. (Here, the parameters are given as wave numbers. For scaling of additional coefficients, see Refs. [36–38].) Thus the absolute sensitivity of a particular state to variation in μ is given by

$$\frac{1}{hc}\frac{\partial E}{\partial(\ln\mu)} = -\tfrac{1}{2}\omega_e\left(v+\tfrac{1}{2}\right) + \omega_e x_e\left(v+\tfrac{1}{2}\right)^2 - B_e J(J+1). \tag{5}$$

Transitions between different vibrational states will generally yield higher sensitivity both because ω_e tends to be larger than B_e and because selection rules preclude transitions between states of vastly different J. The first term in Eq. (5) shows a linear growth in sensitivity with vibrational state. For higher states, the opposite sign of the second term slows the growth. The vibrational states return to no sensitivity near the dissociation limit. As was pointed out in Refs. [16,35], the peak sensitivity is approximately 1/4 of the dissociation energy and occurs for vibrational states with energies approximately 3/4 of the dissociation limit.

Vibrational selection rules typically preclude direct transitions between low- and high-sensitivity states within the same electronic state. To alleviate this restriction, Zelevinsky *et al.* [16] proposed driving stimulated Raman transitions via an excited electronic state and suggested Sr_2 as a candidate molecule. DeMille *et al.* [35] suggested transitions between different electronic states. The linewidth for such a transition can still be narrow if the interelectronic transition is forbidden, for example, by spin selection rules. DeMille *et al.* emphasize the practical advantage of choosing transitions with high relative sensitivity and identify Cs_2 as a candidate molecule with a near degeneracy between vibrational states in different-multiplicity electronic states.

Because the maximum sensitivity is proportional to the potential depth, one should look for experimentally viable routes in deeply bound molecules. Kajita *et al.* [17–19] have identified several vibrational transitions in the N_2^+ molecule that are accessible via two-photon transitions. We propose O_2^+ as a candidate molecule with several accessible transitions that are 50–75 times more sensitive than those in prior proposals with photoassociated molecules. Indeed, even the energy difference between the O_2^+ $X\,^2\Pi_g$ ground and first-excited vibrational states has several times the absolute sensitivity of the transitions proposed in Refs. [16,35]. Because they are both deeply bound, the sensitivities in O_2^+ are comparable to those in N_2^+, though the most sensitive transition we propose is 2–6 times more sensitive than those identified in Refs. [17–19]. Additionally, there are accidental degeneracies in O_2^+ between the 21st and 22nd excited vibrational states of the $X\,^2\Pi_g$ state and $v = 0,1$ of the $a\,^4\Pi_u$ state. Several transitions between these states are likely to have energies in the microwave range. Spin-orbit coupling between $a\,^4\Pi_u$ and the nearby $A\,^2\Pi_u$ state should allow the driving of these nominally spin-forbidden transitions [39].

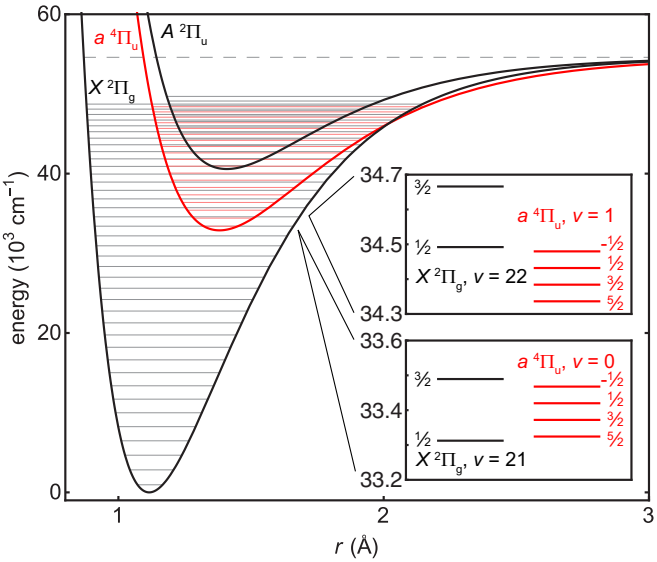

FIG. 1. Potential curves (in the Morse approximation) for the X, a, and A states of O_2^+. The horizontal lines indicate the measured energies of vibrational states [26–28]. The inset shows the doublet-X and quartet-a levels discussed in the text, including spin-orbit splittings. The labels on each fine-structure level indicate Ω in the case (a) (low-J) limit.

The lowest molecular potentials of O_2^+ have been studied for some time. Figure 1 plots the $X\,^2\Pi_g$, $a\,^4\Pi_u$, and $A\,^2\Pi_u$ potentials. The vibrational state energies have been measured up to $v = 38$ for the X state [24,26], $v = 18$ for the a state [25,28], and $v = 12$ for the A state [27]. By use of the resulting molecular parameters as well as Eq. (5), we calculate each vibrational level's sensitivity to variation in μ. These sensitivities, $\partial E_v/\partial(\ln\mu)$, are plotted in Fig. 2. The values plotted in the figure are calculated using a Morse approximation for the potential [36]. For the particular transitions proposed herein, the sensitivity calculated from the Morse potential and from the

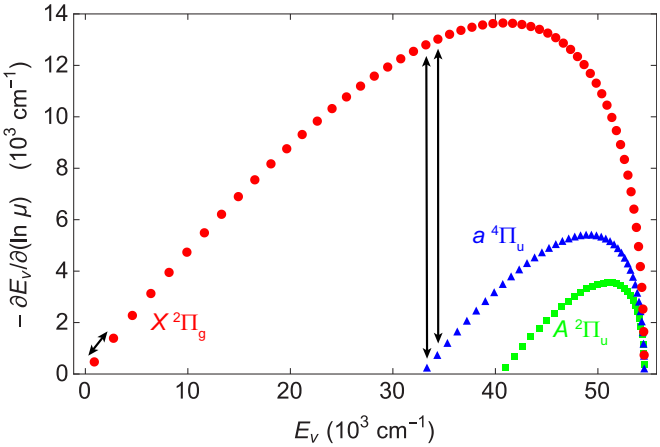

FIG. 2. Absolute sensitivity of vibrational states in the X, a, and A potentials, calculated using the Morse approximation. The arrows indicate the proposed transitions.

measured molecular parameters agree to better than 0.5%. The relevant coefficients are included in the Supplemental Material [40].

The X state's high ω_e means that even the lowest vibrational transitions are quite sensitive to variation in μ. The transition $|X,v=0\rangle \leftrightarrow |X,v=1\rangle$, has a sensitivity of $\frac{1}{2\pi c}\frac{\partial\omega}{\partial(\ln\mu)} = 920\ \mathrm{cm}^{-1} = 28\ \mathrm{THz}/c$ and an energy difference $\Delta E/(hc) = 1873\ \mathrm{cm}^{-1} = 1/(5339\ \mathrm{nm})$. Because $O_2{}^+$ is nonpolar, this transition is $E1$ forbidden but proceeds as an electric quadrupole ($E2$) transition. Its natural linewidth is thus extremely narrow and any experimental linewidth will be limited by technical noise (e.g., laser linewidth) or probe time. An experiment driving the lowest vibrational transitions with two Raman lasers has been proposed in $N_2{}^+$ [17]. The $N_2{}^+$ ground-state $v=0 \leftrightarrow 1$ electric-quadrupole transition has been driven directly with a quantum cascade laser [41]. Similar techniques could be applied to $O_2{}^+$.

Given the absolute sensitivity, we can use Eq. (2) to estimate the achievable statistical precision of a $v=0 \leftrightarrow 1$ measurement. Assuming a probe time equal to Γ^{-1} and minimal experimental dead time, the total number of measurements scales linearly in the total measurement duration τ as $M=\tau\Gamma$. If the signal-to-noise ratio is limited by quantum projection noise [42], then $S/\delta S = \sqrt{N}$, where N is the number of independent molecules probed per experimental run. The statistical precision would then be $\delta\omega \sim \sqrt{\Gamma/(N\tau)}$. With a $\Gamma/(2\pi) = 1$ Hz linewidth, the lowest vibrational transition should be able to achieve $\delta\mu/\mu \sim 1.4\times10^{-14}/\sqrt{N(\tau/\mathrm{s})}$ or of order 5×10^{-17} in 1 day with one molecule.

To enhance sensitivity, one could measure the energy difference between vibrational states near the middle of the potential and those near the bottom or near dissociation. With a potential as deep as $O_2{}^+$, driving such a transition with two Raman lasers becomes challenging. Directly driving the quadrupole overtone transitions suffers from very small quadrupole moments for large Δv. Driving them as two-photon transitions (as proposed for $N_2{}^+$ in Ref. [19]) is a plausible way forward. In the case of $O_2{}^+$, accidental degeneracies between different electronic potentials provide high sensitivity with a relatively low-energy difference. Here, two high-sensitivity states $|X\,^2\Pi_g, v=21{,}22\rangle$ are nearly degenerate with two low-sensitivity states $|a\,^4\Pi_u, v=0{,}1\rangle$. Figure 1 (inset) shows the overlap, including spin-orbit splitting. Because the rotational coefficients of these two states are slightly different, the degeneracy may in some sense be "tuned" by choosing an appropriate J and ΔJ. The absolute sensitivity of the $|X,v''=21\rangle \leftrightarrow |a,v'=0\rangle$ transition is $12\,600\ \mathrm{cm}^{-1} = 378\ \mathrm{THz}/c$; that of the $|X,v''=22\rangle \leftrightarrow |a,v'=1\rangle$ transition is $12\,300\ \mathrm{cm}^{-1} = 369\ \mathrm{THz}/c$. Depending on the particular J and ΔJ, sensitivity contributions from the B_e coefficient may be of order $100\ \mathrm{cm}^{-1}$.

Using measured molecular parameters for the X and a states [22,24–26], we make an effective Hamiltonian [43] and calculate the energies and eigenstates of the individual J states within the relevant vibrational states [40]. We calculate all transition energies with $\Delta J = 0, \pm 1$ and $|\Delta E|/(hc) < 10\ \mathrm{cm}^{-1} = 300\ \mathrm{GHz}/c$. Figure 3 plots the results, which are tabulated in the Supplemental Material [40]. As can be seen, many energies lie in a range where radio-frequency and microwave techniques may be used. The relatively lower

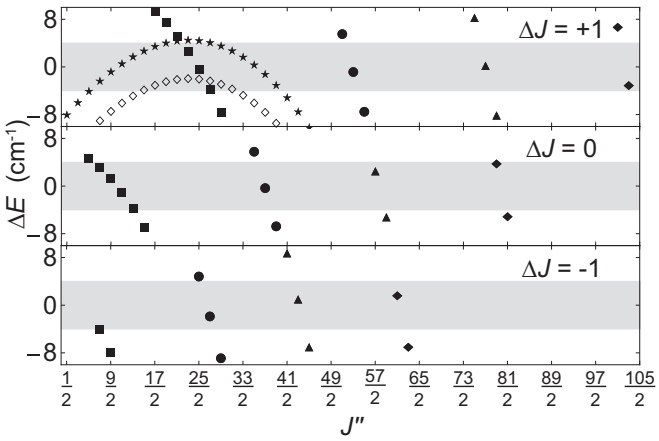

FIG. 3. Near degeneracy of X and a states. Transitions are plotted from $|X\,F_2, v''=21, J''\rangle$ (open) or $|X\,F_1, v''=21, J''\rangle$ (solid) to $|a\,F_1, v'=0, J'\rangle$ (■), F_2 (●), F_3 (▲), or F_4 (◆). The $|X\,F_1, v''=22, J''\rangle \leftrightarrow |a\,F_4, v'=1, J'\rangle$ transitions are plotted with ★. The separate plots indicate $\Delta J = J''-J' = -1$, 0, or +1. Gray bands show a $\pm4\ \mathrm{cm}^{-1}$ uncertainty range. By convention [36,43], the F_i indicate the energy order of the eigenstates for a given J with F_1 having the lowest energy.

transition frequencies relax the demands on relative accuracy while maintaining high absolute sensitivity. The uncertainties on the calculated transition energies are 3–5 cm^{-1}, but they are highly correlated such that even if these particular transitions are no longer within $10\ \mathrm{cm}^{-1}$, others will be.

While transitions between the doublet-X and quartet-a states are spin forbidden, spin-orbit mixing of the $a\,^4\Pi_u$ and $A\,^2\Pi_u$ states ($7625\ \mathrm{cm}^{-1}$ apart) provides sufficient coupling. This mixing also dominates the decay of the a state and thus the linewidth of our proposed transitions. With an estimate of the mixing and the known 690 ns lifetime of the A state [44], we can calculate the linewidth of each transition. Only the $a\,^4\Pi_{1/2,u}$ and $a\,^4\Pi_{3/2,u}$ substates couple to the A state, so we use our effective Hamiltonian to calculate the projection of each eigenstate in the Hund's case (a) basis. A similar technique was used in Ref. [44] to explain a-state-lifetime data. They used $72\ \mathrm{cm}^{-1}$ as an *ab initio* calculated estimate of the matrix elements $\langle a\,^4\Pi_{1/2,u}|H_{\mathrm{SO}}|A\,^2\Pi_{1/2,u}\rangle$ and $\langle a\,^4\Pi_{3/2,u}|H_{\mathrm{SO}}|A\,^2\Pi_{3/2,u}\rangle$, and we do so as well. (Ref. [45] calculates a similar value for these matrix elements.) The transition linewidths fall in the range $\Gamma/(2\pi) = 0.07$–10 Hz [40]. With the same assumptions as before, a 1-Hz-linewidth transition should be able to achieve a statistical precision of $\delta\mu/\mu \sim 1.1\times10^{-15}/\sqrt{N(\tau/\mathrm{s})}$ or of order 4×10^{-18} in 1 day with one molecule.

When estimating the transition dipole moment, the same mixing of a and A states and spin-orbit matrix elements apply. Because the a and A states have similar equilibrium bond lengths, the coupling of $|X,v''\rangle$ to $|a,v'\rangle$ is primarily through a single vibrational state $|A,v'\rangle$. By use of Rydberg-Klein-Rees (RKR) potential curves generated from the data in Refs. [26,27], we calculate [46] the Franck-Condon factor between $|X,v''=21\rangle$ and $|A,v'=0\rangle$ to be 1.8×10^{-6}. This value agrees to within 15% with a prior published value [47] that relied on older spectroscopy data. The electronic

transition moment between $|X,v''=21\rangle$ and $|A,v'=0\rangle$ has been calculated to be $0.503ea_0$ [47]. Combining these elements with our case (a) eigenstates, we estimate the transition dipole moment of these transitions to be of order $10^{-6}ea_0$. A typical transition could be driven with a Rabi frequency approximately the same as its linewidth by use of a microwave electric field of order 10–100 V/m.

We have identified techniques for producing and analyzing the states of O_2^+. Rovibrationally selected O_2^+ molecules have been produced in the $X\,^2\Pi_g$ state with $v=0,1$, and J up to $\frac{51}{2}$ [48]. The production is via resonance-enhanced multiphoton ionization (REMPI) with the selection coming from use of the $d\,^1\Pi_g$ Rydberg state in neutral O_2 [49]. Excitation to the Rydberg state requires two photons in the range 296.5–303.5 nm, and ionization requires a third photon, which could be at the same wavelength. Transfer from $|X,v=0\rangle$ to $|a,v=0\rangle$ could be driven coherently with a laser of wavelength 308 nm. This transition is allowed through the same $a-A$ spin-orbit mixing. The $|X,v=0\rangle \leftrightarrow |A,v=0\rangle$ transition has an electric dipole moment $0.192ea_0$ [47] and Franck-Condon factor 1.7×10^{-6}. A 1-mW laser focused to 50 μm (intensity 2.5×10^5 W/m^2) should produce a Rabi frequency of order 100 Hz.

Detection of the state could be done by driving from $a\,^4\Pi_u$ to $b\,^4\Sigma_g^-$, which has predissociation states at higher vibrational levels [50]. Any population in the $|X,v=21\rangle$ state would not be transferred to the b state. While preliminary measurements could take place in a beam, trapping O_2^+ and sympathetic cooling to a Coulomb crystal with cotrapped atomic ions would allow longer probe times and eliminate first-order Doppler shifts. Trapping only a few atoms and molecules could enable nondestructive detection via quantum logic spectroscopy [51,52]. Such detection could increase the duty cycle by reducing the need to reload ions and would reduce systematic effects associated with micromotion in a radio-frequency trap [53], though it may reduce the statistical limit because fewer molecules would be probed per experiment.

In conclusion, we have identified two routes in the O_2^+ molecular ion to a high-sensitivity search for present-day variation in the proton-to-electron mass ratio. The highest sensitivity comes from an accidental degeneracy between excited vibrational levels of the X state and the lowest vibrational levels of the a state. We note that spin-orbit-coupling energies scale as $\sim\alpha^2$ [11,54] such that any transition between different fine-structure states should be sensitive to α variation in addition to μ variation. A thorough analysis of the systematic effects is an important next step.

We note that there is another set of degeneracies among the O_2^+ $|X,v=27$–$30\rangle$, $|a,v=7$–$10\rangle$, and $|A,v=0$–$2\rangle$ states [40]. The direct overlap with the A state would require a more extensive linewidth calculation than described here. It is also likely that such degeneracies exist in other molecules. Some homonuclear molecules with deep electronic-ground-state potentials and different-multiplicity potentials dipping within them include Te_2 [55], Br_2, Ge_2, and I_2^+ [56]. The heavier of these tend to have smaller vibrational splittings, which increase the likelihood of a degeneracy. It is possible that similar transitions can be found among the infrared-inactive vibrational modes of deeply bound nonpolar polyatomic molecules.

This material is based upon work supported by the NSF under Grant CAREER PHY-1255170 and the Research Corporation for Science Advancement.

[1] J.-P. Uzan, The fundamental constants and their variation: Observational and theoretical status, Rev. Mod. Phys. **75**, 403 (2003).

[2] Y. V. Stadnik and V. V. Flambaum, Can Dark Matter Induce Cosmological Evolution of the Fundamental Constants of Nature? Phys. Rev. Lett. **115**, 201301 (2015).

[3] N. Kanekar, Constraining changes in the proton-electron mass ratio with inversion and rotation lines, Astrophys. J. Lett. **728**, L12 (2011).

[4] J. Bagdonaite, M. Daprà, P. Jansen, H. L. Bethlem, W. Ubachs, S. Muller, C. Henkel, and K. M. Menten, Robust Constraint on a Drifting Proton-to-Electron Mass Ratio at $z=0.89$ from Methanol Observation at Three Radio Telescopes, Phys. Rev. Lett. **111**, 231101 (2013).

[5] W. Ubachs, J. Bagdonaite, E. J. Salumbides, M. T. Murphy, and L. Kaper, Colloquium: Search for a drifting proton-electron mass ratio from H_2, Rev. Mod. Phys. **88**, 021003 (2016).

[6] R. M. Godun, P. B. R. Nisbet-Jones, J. M. Jones, S. A. King, L. A. M. Johnson, H. S. Margolis, K. Szymaniec, S. N. Lea, K. Bongs, and P. Gill, Frequency Ratio of Two Optical Clock Transitions in $^{171}Yb^+$ and Constraints on the Time Variation of Fundamental Constants, Phys. Rev. Lett. **113**, 210801 (2014).

[7] N. Huntemann, B. Lipphardt, Chr. Tamm, V. Gerginov, S. Weyers, and E. Peik, Improved Limit on a Temporal Variation of m_p/m_e from Comparisons of Yb^+ and Cs Atomic Clocks, Phys. Rev. Lett. **113**, 210802 (2014).

[8] V. V. Flambaum and A. F. Tedesco, Dependence of nuclear magnetic moments on quark masses and limits on temporal variation of fundamental constants from atomic clock experiments, Phys. Rev. C **73**, 055501 (2006).

[9] S. Schiller and V. Korobov, Tests of time independence of the electron and nuclear masses with ultracold molecules, Phys. Rev. A **71**, 032505 (2005).

[10] C. Chin and V. V. Flambaum, Enhanced Sensitivity to Fundamental Constants in Ultracold Atomic and Molecular Systems Near Feshbach Resonances, Phys. Rev. Lett. **96**, 230801 (2006).

[11] V. V. Flambaum and M. G. Kozlov, Enhanced Sensitivity to the Time Variation of the Fine-Structure Constant and m_p/m_e in Diatomic Molecules, Phys. Rev. Lett. **99**, 150801 (2007).

[12] L. D. Carr, D. DeMille, R. V. Krems, and J. Ye, Cold and ultracold molecules: Science, technology, and applications, New J. Phys. **11**, 055049 (2009).

[13] C. Chin, V. V. Flambaum, and M. G. Kozlov, Ultracold molecules: New probes on the variation of fundamental constants, New J. Phys. **11**, 055048 (2009).

[14] P. Jansen, H. L. Bethlem, and W. Ubachs, Perspective: Tipping the scales: Search for drifting constants from molecular spectra, J. Chem. Phys. **140**, 010901 (2014).

[15] A. Shelkovnikov, R. J. Butcher, C. Chardonnet, and A. Amy-Klein, Stability of the Proton-to-Electron Mass Ratio, Phys. Rev. Lett. **100**, 150801 (2008).

[16] T. Zelevinsky, S. Kotochigova, and J. Ye, Precision Test of Mass-Ratio Variations with Lattice-Confined Ultracold Molecules, Phys. Rev. Lett. **100**, 043201 (2008).

[17] M. Kajita, G. Gopakumar, M. Abe, M. Hada, and M. Keller, Test of m_p/m_e changes using vibrational transitions in N_2^+, Phys. Rev. A **89**, 032509 (2014).

[18] M. Kajita, N_2^+ quadrupole transitions with small Zeeman shift, Phys. Rev. A **92**, 043423 (2015).

[19] M. Kajita, Evaluation of variation in (m_p/m_e) from the frequency difference between the $^{15}N_2^+$ and ^{87}Sr transitions, Appl. Phys. B **122**, 203 (2016).

[20] P. H. Krupenie, The spectrum of molecular oxygen, J. Phys. Chem. Ref. Data **1**, 423 (1972).

[21] P. C. Cosby, J.-B. Ozenne, J. T. Moseley, and D. L. Albritton, High-resolution photofragment spectroscopy of the O_2^+ $b\,^4\Sigma_g^-(v'=3,4,5) \leftarrow a\,^4\Pi_u(v'=3,4,5)$ first negative system using coaxial dye-laser and velocity-tuned ion beams, J. Mol. Spectrosc. **79**, 203 (1980).

[22] J. C. Hansen, J. T. Moseley, and P. C. Cosby, High-resolution photofragment spectroscopy of the O_2^+ $b\,^4\Sigma_g^-(v'=5-8) \leftarrow a\,^4\Pi_u(v''=6-9)$ first negative system, J. Mol. Spectrosc. **98**, 48 (1983).

[23] J. A. Coxon and M. P. Haley, Rotational analysis of the $A\,^2\Pi_u \rightarrow X\,^2\Pi_g$ second negative band system of $^{16}O_2^+$, J. Mol. Spectrosc. **108**, 119 (1984).

[24] W. Kong and J. W. Hepburn, Rotationally resolved threshold photoelectron spectroscopy of O_2 using coherent XUV: Formation of vibrationally excited ions in the Franck-Condon gap, Can. J. Phys. **72**, 1284 (1994).

[25] W. Kong and J. W. Hepburn, PFI-ZEKE spectroscopy using coherent vacuum UV: $O_2^+(a\,^4\Pi_u) \leftarrow O_2(X\,^3\Sigma_g^-)$, Int. J. Mass Spectrom. Ion Processes **159**, 27 (1996).

[26] Y. Song, M. Evans, C. Y. Ng, C.-W. Hsu, and G. K. Jarvis, Rotationally resolved pulsed field ionization photoelectron bands of $O_2^+(X\,^2\Pi_{1/2,3/2g}, v^+ = 0$–$38)$ in the energy range of 12.05–18.15 eV, J. Chem. Phys. **111**, 1905 (1999).

[27] Y. Song, M. Evans, C. Y. Ng, C.-W. Hsu, and G. K. Jarvis, Rotationally resolved pulsed-field ionization photoelectron bands of $O_2^+(A\,^2\Pi_u, v^+ = 0$–$12)$ in the energy range of 17.0–18.2 eV, J. Chem. Phys. **112**, 1271 (2000).

[28] Y. Song, M. Evans, C. Y. Ng, C.-W. Hsu, and G. K. Jarvis, Rotationally resolved pulsed field ionization photoelectron bands of $O_2^+(a\,^4\Pi_u, v^+ = 0$–$18)$ in the energy range of 16.0–18.0 eV, J. Chem. Phys. **112**, 1306 (2000).

[29] D. G. Fedorov, M. Evans, Y. Song, M. S. Gordon, and C. Y. Ng, An experimental and theoretical study of the spin-orbit interaction for CO^+ $(A\,^2\Pi_{3/2,1/2}, v^+ = 0$–$41)$ and O_2^+ $(X\,^2\Pi_{3/2,1/2g}, v^+ = 0$–$38)$, J. Chem. Phys. **111**, 6413 (1999).

[30] D. G. Fedorov, M. S. Gordon, Y. Song, and C. Y. Ng, Theoretical study of spin-orbit coupling constants for O_2^+ $(A\,^2\Pi_{3/2,1/2u}, v^+ = 0$–$17$ and $a\,^4\Pi_{5/2,3/2,1/2,-1/2u}, v^+ = 0$–$25)$, J. Chem. Phys. **115**, 7393 (2001).

[31] X. Zhang, D. Shi, J. Sun, and Z. Zhu, MRCI study of spectroscopic and molecular properties of $X^2\Pi_g$, $a^4\Pi_u$, $A^2\Pi_u$, $b^4\Sigma_g^-$, $D^2\Delta_g$ and $B^2\Sigma_g^-$ electronic states of O_2^+ ion, Mol. Phys. **109**, 1627 (2011).

[32] M. Magrakvelidze, C. M. Aikens, and U. Thumm, Dissociation dynamics of diatomic molecules in intense laser fields: A scheme for the selection of relevant adiabatic potential curves, Phys. Rev. A **86**, 023402 (2012).

[33] H. Liu, D. Shi, J. Sun, and Z. Zhu, Accurate theoretical investigations of the 20 $\Lambda - S$ and 58 Ω states of O_2^+ cation including spin-orbit coupling effect, Mol. Phys. **113**, 120 (2015).

[34] R. W. Schunk and A. F. Nagy, Ionospheres of the terrestrial planets, Rev. Geophys. Space Phys. **18**, 813 (1980).

[35] D. DeMille, S. Sainis, J. Sage, T. Bergeman, S. Kotochigova, and E. Tiesinga, Enhanced Sensitivity to Variation of m_e/m_p in Molecular Spectra, Phys. Rev. Lett. **100**, 043202 (2008).

[36] G. Herzberg, *Molecular Spectra and Molecular Structure, Vol. I: Spectra of Diatomic Molecules* (Van Nostrand, New York, 1950).

[37] K. Beloy, M. G. Kozlov, A. Borschevsky, A. W. Hauser, V. V. Flambaum, and P. Schwerdtfeger, Rotational spectrum of the molecular ion NH^+ as a probe for α and m_e/m_p variation, Phys. Rev. A **83**, 062514 (2011).

[38] L. F. Pašteka, A. Borschevsky, V. V. Flambaum, and P. Schwerdtfeger, Search for the variation of fundamental constants: Strong enhancements in $X\,^2\Pi$ cations of dihalogens and hydrogen halides, Phys. Rev. A **92**, 012103 (2015).

[39] H. Lefebvre-Brion and R. W. Field, *The Spectra and Dynamics of Diatomic Molecules* (Elsevier, Amsterdam, 2004).

[40] See Supplemental Material at http://link.aps.org/supplemental/10.1103/PhysRevA.94.050101 for additional calculations, data tables, and figures.

[41] M. Germann, X. Tong, and S. Willitsch, Observation of electric-dipole-forbidden infrared transitions in cold molecular ions, Nat. Phys. **10**, 820 (2014).

[42] W. M. Itano, J. C. Bergquist, J. J. Bollinger, J. M. Gilligan, D. J. Heinzen, F. L. Moore, M. G. Raizen, and D. J. Wineland, Quantum projection noise: Population fluctuations in two-level systems, Phys. Rev. A **47**, 3554 (1993).

[43] J. Brown and A. Carrington, *Rotational Spectroscopy of Diatomic Molecules* (Cambridge University Press, Cambridge, U.K., 2003).

[44] C.-H. Kuo, T. Wyttenbach, C. G. Beggs, P. R. Kemper, and M. T. Bowers, Radiative lifetimes of metatable $O_2^+(a\,^4\Pi_u)$ and $NO^+(a\,^3\Sigma^+)$, J. Chem. Phys. **92**, 4849 (1990).

[45] B. F. Minaev, Calculation of the $a\,^4\Pi_u - X\,^2\Pi_g$ transition intensity in the O_2^+ ion, Opt. Spektrosk. **80**, 407 (1996).

[46] R. J. Le Roy, *RKR1 2.1: A Computer Program Implementing the First-Order RKR Method for Determining Diatomic Molecule Potential Energy Functions*, University of Waterloo Chemical Physics Research Report No. CP-657R (2016); *LEVEL 8.2: A Computer Program for Solving the Radial Schrödinger Equation for Bound and Quasibound Levels*, University of Waterloo Chemical Physics Research Report No. CP-668 (2014), see http://leroy.waterloo.ca/programs/.

[47] F. R. Gilmore, R. R. Laher, and P. J. Espy, Franck-Condon factors, r-centroids, electronic transition moments, and Einstein coefficients for many nitrogen and oxygen band systems, J. Phys. Chem. Ref. Data **21**, 1005 (1992).

[48] A. Dochain and X. Urbain, Production of a rovibrationally selected O_2^+ beam for dissociative recombination studies, EPJ Web Conf. **84**, 05001 (2015).

[49] A. Sur, R. S. Friedman, and P. J. Miller, Rotational dependence of the Rydberg-valence interactions in the $^1\Pi_g$ states of molecular oxygen, J. Chem. Phys. **94**, 1705 (1991).

[50] J. C. Hansen, J. T. Moseley, A. L. Roche, and P. C. Cosby, Lifetimes and predissociation mechanisms of O_2^+ $b\,^4\Sigma_g^-(v = 5–8)$, J. Chem. Phys. **77**, 1206 (1982).

[51] P. O. Schmidt, T. Rosenband, C. Langer, W. M. Itano, J. C. Bergquist, and D. J. Wineland, Spectroscopy using quantum logic, Science **309**, 749 (2005).

[52] F. Wolf, Y. Wan, J. C. Heip, F. Gerbert, C. Shi, and P. O. Schmidt, Nondestructive state detection for quantum logic spectroscopy of molecular ions, Nature (London) **530**, 457 (2016).

[53] D. J. Berkeland, J. D. Miller, J. C. Bergquist, W. M. Itano, and D. J. Wineland, Minimization of ion micromotion in a Paul trap, J. Appl. Phys. **83**, 5025 (1998).

[54] K. Beloy, A. Borschevsky, V. V. Flambaum, and P. Schwerdtfeger, Effect of α variation on a prospective experiment to detect variation of m_e/m_p in diatomic molecules, Phys. Rev. A **84**, 042117 (2011).

[55] D. DeMille, M. G. Kozlov, and S. Kotochigova (private communication).

[56] K. Balasubramanian, Spectroscopic constants and potential energy curves of heavy p-block dimers and trimers, Chem. Rev. **90**, 93 (1990).

Supplemental Material: High sensitivity to proton-to-electron mass ratio variation in O_2^+

D. Hanneke, R. A. Carollo, and D. A. Lane
Physics & Astronomy Department, Amherst College, Amherst, Massachusetts 01002, USA

SENSITIVITY CALCULATIONS

Equation (5) in the main text gives the absolute sensitivity of a particular rovibration state in terms of molecular parameters. Table SI lists the relevant parameters for the $X\,^2\Pi_g$, $a\,^4\Pi_u$, and $A\,^2\Pi_u$ states. We provide the lowest anharmonic coefficients $\omega_e x_e$ both as measured molecular parameters and as calculated parameters in the Morse-potential approximation [S1]. The calculated coefficients rely on each state's potential depth, which we calculate from the measured dissociation limit (18.733(3) eV [S2]) and each state's electronic energy T_e. For the levels of interest, the sensitivity coefficients agree to better than 0.5 % with either anharmonic coefficient. For example, $X\,^2\Pi_g, v = 21$, has $\frac{1}{hc}\frac{\partial E}{\partial(\ln\mu)} = -12\,860\ \mathrm{cm}^{-1}$ using the measured $\omega_e x_e$ and $-12\,800\ \mathrm{cm}^{-1}$ using the calculated value. The main text's Fig. 2 uses the Morse-potential values.

TABLE SI. Coefficients used in sensitivity calculations. Uncertainties are shown in parentheses.

state	T_e/cm^{-1}	$\omega_e/\mathrm{cm}^{-1}$	$\omega_e x_e$(measured)/cm^{-1}	$\omega_e x_e$(Morse)/cm^{-1}
$X\,^2\Pi_g$	96496(4)[a]	1906.069(27)[b]	16.5054(84)[b]	16.6363(73)
$a\,^4\Pi_u$	129378.3(3.2)[c]	1035.5190(35)[d]	10.382(23)[d]	12.346(14)
$A\,^2\Pi_u$	137073.2(3.2)[e]	898.10(33)[f]	13.22(15)[f]	14.384(12)

[a] Ref. [S2]
[b] Ref. [S3]
[c] Ref. [S4]
[d] Ref. [S5]
[e] Ref. [S6]
[f] Ref. [S7]

EFFECTIVE HAMILTONIAN

To calculate the energies and eigenstates of the rotational levels in a particular vibrational state, we diagonalize an effective Hamiltonian. See, for example, ref. [S8, Eq. 10.114–10.115]. We include the electronic and vibrational state energy T_v, spin–orbit coupling A_v, and rigid-body rotation B_v. As discussed below, higher-order terms such as centrifugal distortion D_v or Λ-doubling are not necessary at our precision.

Eigenstates in both $X\,^2\Pi_g$ and $a\,^4\Pi_u$ are written in the Hund's case-(a) basis:

$$c_{3/2}\left|{}^2\Pi_{3/2}\right\rangle + c_{1/2}\left|{}^2\Pi_{1/2}\right\rangle \tag{S1}$$

$$c_{5/2}\left|{}^4\Pi_{5/2}\right\rangle + c_{3/2}\left|{}^4\Pi_{3/2}\right\rangle + c_{1/2}\left|{}^4\Pi_{1/2}\right\rangle + c_{-1/2}\left|{}^4\Pi_{-1/2}\right\rangle. \tag{S2}$$

In these bases, the effective Hamiltonians are given by

$$H(^2\Pi) = \begin{pmatrix} T_v + \frac{A_v}{2} + B_v\left[J(J+1) - \frac{7}{4}\right] & -B_v\sqrt{J(J+1) - \frac{3}{4}} \\ -B_v\sqrt{J(J+1) - \frac{3}{4}} & T_v - \frac{A_v}{2} + B_v\left[J(J+1) + \frac{1}{4}\right] \end{pmatrix} \tag{S3}$$

and

$$H(^4\Pi) = \begin{pmatrix} T_v+\frac{3A_v}{2}+B_v\left[J(J+1)-\frac{19}{4}\right] & -\sqrt{3}B_v\sqrt{J(J+1)-\frac{15}{4}} & 0 & 0 \\ -\sqrt{3}B_v\sqrt{J(J+1)-\frac{15}{4}} & T_v+\frac{A_v}{2}+B_v\left[J(J+1)+\frac{5}{4}\right] & -2B_v\sqrt{J(J+1)-\frac{3}{4}} & 0 \\ 0 & -2B_v\sqrt{J(J+1)-\frac{3}{4}} & T_v-\frac{A_v}{2}+B_v\left[J(J+1)+\frac{13}{4}\right] & -\sqrt{3}B_v(J+\frac{1}{2}) \\ 0 & 0 & -\sqrt{3}B_v(J+\frac{1}{2}) & T_v-\frac{3A_v}{2}+B_v\left[J(J+1)+\frac{5}{4}\right] \end{pmatrix}. \tag{S4}$$

The top-left component is the one with $\Omega = 3/2$ and $5/2$, respectively.

The parameters used in these Hamiltonians are listed in Table SII. Although some identified transitions occur at fairly high J, the contributions of the D_v coefficients are not important at the few-cm^{-1} scale. The D_v coefficients for the $|a\,^4\Pi_u, v' = 0, 1\rangle$ states are $5.0455(189)\times10^{-6}$ cm^{-1} and $5.0567(176)\times10^{-6}$ cm^{-1}, respectively [S5]. We extrapolate the D_v coefficients of the $X\,^2\Pi_g$ state from merged parameters in ref. [S7] to obtain $D_{21} = 5.43(85)\times10^{-6}$ cm^{-1} and $D_{22} = 5.34(92)\times10^{-6}$ cm^{-1}. Even at the higher J's, the contributions from D_v cancel to be consistent with zero with uncertainties of a few times 0.1 cm^{-1}.

TABLE SII. Coefficients used in energy calculations. Uncertainties are shown in parentheses.

state	T_v/cm^{-1}	A_v/cm^{-1}	B_v/cm^{-1}
$X\,^2\Pi_g, v = 21$	129896.9(2.0)[a]	177.0(1.0)[b]	1.25(3)[b]
$X\,^2\Pi_g, v = 22$	131075(5)[b]	174.0(1.0)[b]	1.25(1)[b]
$a\,^4\Pi_u, v = 0$	129892(2)[c]	−47.7927(19)[d]	1.096990(26)[d]
$a\,^4\Pi_u, v = 1$	130904(2)[c]	−47.7997(21)[d]	1.081532(18)[d]

[a] Ref. [S3]
[b] Ref. [S2]
[c] Ref. [S9]
[d] Ref. [S5]

TABLES OF NEAR-DEGENERACIES

Below are tables listing every pair of energy levels with $|\Delta E| < 10$ cm^{-1} and $\Delta J = 0, \pm1$. Also provided are the estimated linewidths and the eigenstate superposition coefficients from diagonalizing the effective Hamiltonians above. The uncertainties in ΔE are 3–6 cm^{-1}. They are highly correlated, however, such that even if these particular transitions are no longer within 10 cm^{-1}, others likely will be. By convention [S1, S8], the F_i indicate the energy order of the eigenstates for a given J with F_1 having the lowest energy. In the case (a) limit, the O_2^+ $X\,^2\Pi_g$ state has $\Omega = \frac{1}{2}$ in F_1 and $\frac{3}{2}$ in F_2, while the $a\,^4\Pi_u$ state has $\Omega = \frac{5}{2}, \frac{3}{2}, \frac{1}{2}, -\frac{1}{2}$ in $F_{1,2,3,4}$.

TABLE SIII: The near-degeneracies $|X\,^2\Pi_g, v'' = 21, J''\rangle$ and $|a\,^4\Pi_u, v' = 0, J'\rangle$, including the eigenstate superposition coefficients.

$X\,^2\Pi_g$	$a\,^4\Pi_u$	J''	J'	ΔE/cm^{-1}	$\frac{\Gamma}{2\pi}$/Hz	$c''_{3/2}$	$c''_{1/2}$	$c'_{5/2}$	$c'_{3/2}$	$c'_{1/2}$	$c'_{-1/2}$
F_2	F_4	$\frac{7}{2}$	$\frac{9}{2}$	−8.88	0.45	−1.00	0.03	−0.00	0.02	−0.20	0.98
F_2	F_4	$\frac{9}{2}$	$\frac{11}{2}$	−7.30	0.63	−1.00	0.04	−0.00	0.03	−0.24	0.97
F_2	F_4	$\frac{11}{2}$	$\frac{13}{2}$	−5.91	0.83	−1.00	0.04	−0.00	0.04	−0.27	0.96
F_2	F_4	$\frac{13}{2}$	$\frac{15}{2}$	−4.71	1.05	−1.00	0.05	−0.01	0.05	−0.30	0.95
F_2	F_4	$\frac{15}{2}$	$\frac{17}{2}$	−3.71	1.28	−1.00	0.06	−0.01	0.07	−0.34	0.94
F_2	F_4	$\frac{17}{2}$	$\frac{19}{2}$	−2.91	1.52	−1.00	0.06	−0.01	0.08	−0.36	0.93
F_2	F_4	$\frac{19}{2}$	$\frac{21}{2}$	−2.32	1.77	−1.00	0.07	−0.01	0.09	−0.39	0.92
F_2	F_4	$\frac{21}{2}$	$\frac{23}{2}$	−1.95	2.02	−1.00	0.08	−0.01	0.11	−0.42	0.90
F_2	F_4	$\frac{23}{2}$	$\frac{25}{2}$	−1.80	2.27	−1.00	0.08	−0.02	0.12	−0.44	0.89
F_2	F_4	$\frac{25}{2}$	$\frac{27}{2}$	−1.88	2.52	−1.00	0.09	−0.02	0.13	−0.46	0.88
F_2	F_4	$\frac{27}{2}$	$\frac{29}{2}$	−2.19	2.76	−1.00	0.10	−0.03	0.15	−0.48	0.86
F_2	F_4	$\frac{29}{2}$	$\frac{31}{2}$	−2.74	3.00	−0.99	0.11	−0.03	0.16	−0.50	0.85
F_2	F_4	$\frac{31}{2}$	$\frac{33}{2}$	−3.54	3.23	−0.99	0.11	−0.03	0.18	−0.51	0.84
F_2	F_4	$\frac{33}{2}$	$\frac{35}{2}$	−4.60	3.45	−0.99	0.12	−0.04	0.19	−0.53	0.83
F_2	F_4	$\frac{35}{2}$	$\frac{37}{2}$	−5.90	3.66	−0.99	0.13	−0.04	0.20	−0.54	0.81
F_2	F_4	$\frac{37}{2}$	$\frac{39}{2}$	−7.47	3.87	−0.99	0.13	−0.05	0.21	−0.55	0.80
F_2	F_4	$\frac{39}{2}$	$\frac{41}{2}$	−9.30	4.07	−0.99	0.14	−0.05	0.23	−0.57	0.79
F_1	F_1	$\frac{7}{2}$	$\frac{5}{2}$	−3.90	0.07	−0.03	−1.00	1.00	0.08	0.00	0.00
F_1	F_1	$\frac{9}{2}$	$\frac{7}{2}$	−7.85	0.16	−0.04	−1.00	0.99	0.12	0.01	0.00

TABLE SIII: (continued)

$X\,^2\Pi_g$	$a\,^4\Pi_u$	J''	J'	$\Delta E/\mathrm{cm}^{-1}$	$\frac{\Gamma}{2\pi}$/Hz	$c''_{3/2}$	$c''_{1/2}$	$c'_{5/2}$	$c'_{3/2}$	$c'_{1/2}$	$c'_{-1/2}$
F_1	F_1	$\frac{5}{2}$	$\frac{5}{2}$	4.79	0.07	−0.02	−1.00	1.00	0.08	0.00	0.00
F_1	F_1	$\frac{7}{2}$	$\frac{7}{2}$	3.32	0.16	−0.03	−1.00	0.99	0.12	0.01	0.00
F_1	F_1	$\frac{9}{2}$	$\frac{9}{2}$	1.43	0.27	−0.04	−1.00	0.99	0.16	0.02	0.00
F_1	F_1	$\frac{11}{2}$	$\frac{11}{2}$	−0.87	0.41	−0.04	−1.00	0.98	0.19	0.02	0.00
F_1	F_1	$\frac{13}{2}$	$\frac{13}{2}$	−3.59	0.57	−0.05	−1.00	0.97	0.23	0.03	0.00
F_1	F_1	$\frac{15}{2}$	$\frac{15}{2}$	−6.71	0.74	−0.06	−1.00	0.97	0.26	0.04	0.00
F_1	F_1	$\frac{17}{2}$	$\frac{19}{2}$	9.42	1.12	−0.06	−1.00	0.95	0.31	0.06	0.01
F_1	F_1	$\frac{19}{2}$	$\frac{21}{2}$	7.57	1.33	−0.07	−1.00	0.94	0.34	0.08	0.01
F_1	F_1	$\frac{21}{2}$	$\frac{23}{2}$	5.34	1.55	−0.08	−1.00	0.93	0.37	0.09	0.01
F_1	F_1	$\frac{23}{2}$	$\frac{25}{2}$	2.72	1.76	−0.08	−1.00	0.92	0.39	0.10	0.02
F_1	F_1	$\frac{25}{2}$	$\frac{27}{2}$	−0.28	1.99	−0.09	−1.00	0.90	0.41	0.11	0.02
F_1	F_1	$\frac{27}{2}$	$\frac{29}{2}$	−3.67	2.21	−0.10	−1.00	0.89	0.43	0.13	0.02
F_1	F_1	$\frac{29}{2}$	$\frac{31}{2}$	−7.42	2.43	−0.11	−0.99	0.88	0.45	0.14	0.03
F_1	F_2	$\frac{25}{2}$	$\frac{23}{2}$	4.95	9.38	−0.09	−1.00	−0.36	0.82	0.44	0.10
F_1	F_2	$\frac{27}{2}$	$\frac{25}{2}$	−1.75	9.16	−0.10	−1.00	−0.39	0.79	0.46	0.11
F_1	F_2	$\frac{29}{2}$	$\frac{27}{2}$	−8.77	8.93	−0.11	−0.99	−0.41	0.76	0.48	0.13
F_1	F_2	$\frac{35}{2}$	$\frac{35}{2}$	5.91	8.04	−0.13	−0.99	−0.48	0.66	0.55	0.18
F_1	F_2	$\frac{37}{2}$	$\frac{37}{2}$	−0.21	7.82	−0.13	−0.99	−0.50	0.63	0.56	0.19
F_1	F_2	$\frac{39}{2}$	$\frac{39}{2}$	−6.63	7.61	−0.14	−0.99	0.51	−0.60	−0.58	−0.21
F_1	F_2	$\frac{51}{2}$	$\frac{53}{2}$	5.66	6.33	−0.18	−0.98	−0.58	0.44	0.62	0.29
F_1	F_2	$\frac{53}{2}$	$\frac{55}{2}$	−0.72	6.18	−0.18	−0.98	−0.59	0.42	0.62	0.30
F_1	F_2	$\frac{55}{2}$	$\frac{57}{2}$	−7.39	6.04	−0.19	−0.98	0.60	−0.40	−0.63	−0.30
F_1	F_3	$\frac{41}{2}$	$\frac{39}{2}$	8.89	7.13	−0.15	−0.99	−0.19	0.57	−0.57	−0.56
F_1	F_3	$\frac{43}{2}$	$\frac{41}{2}$	1.14	6.94	−0.15	−0.99	0.21	−0.58	0.55	0.57
F_1	F_3	$\frac{45}{2}$	$\frac{43}{2}$	−6.87	6.76	−0.16	−0.99	−0.22	0.59	−0.52	−0.58
F_1	F_3	$\frac{57}{2}$	$\frac{57}{2}$	2.66	5.71	−0.20	−0.98	0.29	−0.62	0.37	0.63
F_1	F_3	$\frac{59}{2}$	$\frac{59}{2}$	−5.06	5.58	−0.20	−0.98	−0.30	0.62	−0.35	−0.63
F_1	F_3	$\frac{75}{2}$	$\frac{77}{2}$	8.43	4.74	−0.25	−0.97	0.37	−0.62	0.21	0.66
F_1	F_3	$\frac{77}{2}$	$\frac{79}{2}$	0.36	4.67	−0.25	−0.97	−0.37	0.62	−0.20	−0.66
F_1	F_3	$\frac{79}{2}$	$\frac{81}{2}$	−7.99	4.60	−0.26	−0.97	0.38	−0.62	0.18	0.66
F_1	F_4	$\frac{61}{2}$	$\frac{59}{2}$	1.74	5.45	−0.21	−0.98	−0.09	0.32	−0.63	0.70
F_1	F_4	$\frac{63}{2}$	$\frac{61}{2}$	−6.89	5.57	−0.21	−0.98	0.09	−0.33	0.63	−0.69
F_1	F_4	$\frac{79}{2}$	$\frac{79}{2}$	3.89	6.38	−0.26	−0.97	0.13	−0.39	0.66	−0.63
F_1	F_4	$\frac{81}{2}$	$\frac{81}{2}$	−4.98	6.45	−0.26	−0.96	0.13	−0.39	0.66	−0.63
F_1	F_4	$\frac{101}{2}$	$\frac{103}{2}$	6.82	7.01	−0.31	−0.95	0.16	−0.44	0.67	−0.58
F_1	F_4	$\frac{103}{2}$	$\frac{105}{2}$	−2.97	7.05	−0.31	−0.95	0.17	−0.44	0.67	−0.57

TABLE SIV: The near-degeneracies $|X\,^2\Pi_g, v'' = 22, J''\rangle$ and $|a\,^4\Pi_u, v' = 1, J'\rangle$, including the eigenstate superposition coefficients.

$X\,^2\Pi_g$	$a\,^4\Pi_u$	J''	J'	$\Delta E/\mathrm{cm}^{-1}$	$\frac{\Gamma}{2\pi}/\mathrm{Hz}$	$c''_{3/2}$	$c''_{1/2}$	$c'_{5/2}$	$c'_{3/2}$	$c'_{1/2}$	$c'_{-1/2}$
F_1	F_4	$\frac{1}{2}$	$\frac{3}{2}$	−7.84	0.08	0.00	1.00	0.00	0.00	−0.08	1.00
F_1	F_4	$\frac{3}{2}$	$\frac{5}{2}$	−5.77	0.17	−0.01	−1.00	−0.00	0.01	−0.12	0.99
F_1	F_4	$\frac{5}{2}$	$\frac{7}{2}$	−3.87	0.30	−0.02	−1.00	−0.00	0.01	−0.16	0.99
F_1	F_4	$\frac{7}{2}$	$\frac{9}{2}$	−2.15	0.45	−0.03	−1.00	−0.00	0.02	−0.20	0.98
F_1	F_4	$\frac{9}{2}$	$\frac{11}{2}$	−0.61	0.63	−0.04	−1.00	−0.00	0.03	−0.23	0.97
F_1	F_4	$\frac{11}{2}$	$\frac{13}{2}$	0.75	0.84	−0.04	−1.00	−0.00	0.04	−0.27	0.96
F_1	F_4	$\frac{13}{2}$	$\frac{15}{2}$	1.92	1.06	−0.05	−1.00	−0.00	0.05	−0.30	0.95
F_1	F_4	$\frac{15}{2}$	$\frac{17}{2}$	2.90	1.30	−0.06	−1.00	−0.01	0.06	−0.33	0.94
F_1	F_4	$\frac{17}{2}$	$\frac{19}{2}$	3.67	1.55	−0.06	−1.00	−0.01	0.08	−0.36	0.93
F_1	F_4	$\frac{19}{2}$	$\frac{21}{2}$	4.24	1.80	−0.07	−1.00	−0.01	0.09	−0.39	0.92
F_1	F_4	$\frac{21}{2}$	$\frac{23}{2}$	4.59	2.06	−0.08	−1.00	−0.01	0.10	−0.41	0.91
F_1	F_4	$\frac{23}{2}$	$\frac{25}{2}$	4.73	2.31	−0.09	−1.00	−0.02	0.12	−0.44	0.89
F_1	F_4	$\frac{25}{2}$	$\frac{27}{2}$	4.63	2.57	−0.09	−1.00	−0.02	0.13	−0.46	0.88
F_1	F_4	$\frac{27}{2}$	$\frac{29}{2}$	4.31	2.82	−0.10	−0.99	−0.02	0.14	−0.48	0.87
F_1	F_4	$\frac{29}{2}$	$\frac{31}{2}$	3.74	3.06	−0.11	−0.99	−0.03	0.16	−0.49	0.85
F_1	F_4	$\frac{31}{2}$	$\frac{33}{2}$	2.93	3.30	−0.11	−0.99	−0.03	0.17	−0.51	0.84
F_1	F_4	$\frac{33}{2}$	$\frac{35}{2}$	1.87	3.53	−0.12	−0.99	−0.04	0.18	−0.53	0.83
F_1	F_4	$\frac{35}{2}$	$\frac{37}{2}$	0.56	3.75	−0.13	−0.99	−0.04	0.20	−0.54	0.82
F_1	F_4	$\frac{37}{2}$	$\frac{39}{2}$	−1.01	3.97	−0.13	−0.99	0.04	−0.21	0.55	−0.81
F_1	F_4	$\frac{39}{2}$	$\frac{41}{2}$	−2.85	4.17	−0.14	−0.99	0.05	−0.22	0.56	−0.79
F_1	F_4	$\frac{41}{2}$	$\frac{43}{2}$	−4.95	4.36	−0.15	−0.99	−0.05	0.23	−0.57	0.78
F_1	F_4	$\frac{43}{2}$	$\frac{45}{2}$	−7.32	4.55	−0.15	−0.99	−0.06	0.25	−0.58	0.77
F_1	F_4	$\frac{45}{2}$	$\frac{47}{2}$	−9.97	4.73	−0.16	−0.99	−0.06	0.26	−0.59	0.76

OTHER DEGENERACIES

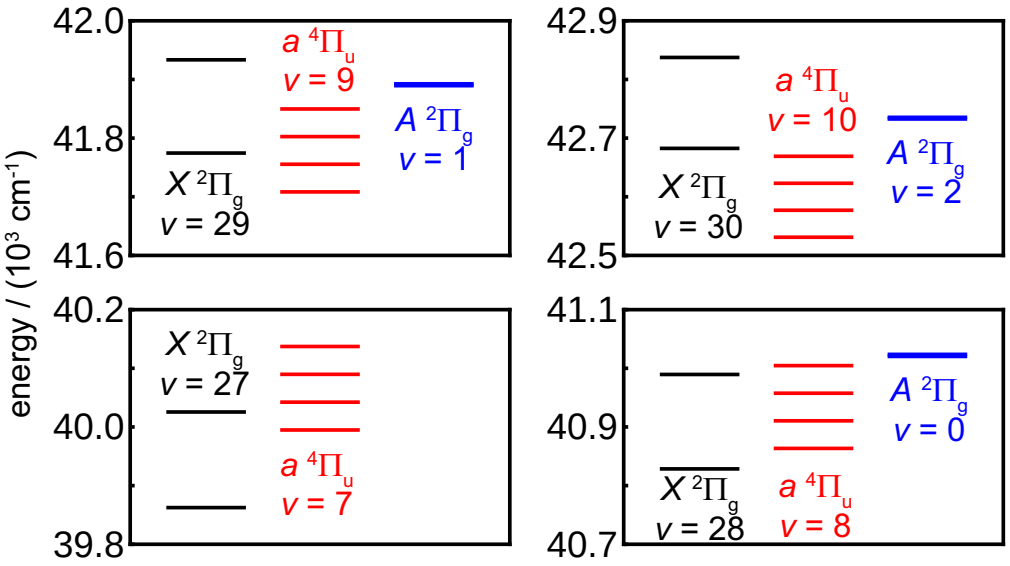

FIG. S1. Overlap of the $X\,^2\Pi_g$, $a\,^4\Pi_u$, and $A\,^2\Pi_u$ states near $|X, v = 27\text{–}30\rangle$. The levels are calculated from refs. [S2, S4, S6]. Note that the A state's spin-orbit constant is small enough that the doublet splitting is not visible at this scale.

[S1] Gerhard Herzberg, *Molecular Spectra and Molecular Structure, Vol. I: Spectra of Diatomic Molecules* (D. Van Nostrand Co., 1950).

[S2] Y. Song, M. Evans, C. Y. Ng, C.-W. Hsu, and G. K. Jarvis, "Rotationally resolved pulsed field ionization photoelectron bands of $O_2^+(X\,^2\Pi_{1/2,3/2g}, v^+ = 0-38)$ in the energy range of $12.05 - 18.15$ eV," J. Chem. Phys. **111**, 1905–1916 (1999).

[S3] W. Kong and J. W. Hepburn, "Rotationally resolved threshold photoelectron spectroscopy of O_2 using coherent XUV: formation of vibrationally excited ions in the Franck–Condon gap," Can. J. Phys. **72**, 1284–1293 (1994).

[S4] Y. Song, M. Evans, C. Y. Ng, C.-W. Hsu, and G. K. Jarvis, "Rotationally resolved pulsed field ionization photoelectron bands of $O_2^+(a\,^4\Pi_u, v^+ = 0-18)$ in the energy range of $16.0 - 18.0$ eV," J. Chem. Phys. **112**, 1306–1315 (2000).

[S5] J. C. Hansen, J. T. Moseley, and P. C. Cosby, "High-resolution photofragment spectroscopy of the $O_2^+\ b\,^4\Sigma_g^-(v' = 5-8) \leftarrow a\,^4\Pi_u(v'' = 6-9)$ first negative system," J. Mol. Spec. **98**, 48–63 (1983).

[S6] Y. Song, M. Evans, C. Y. Ng, C.-W. Hsu, and G. K. Jarvis, "Rotationally resolved pulsed-field ionization photoelectron bands of $O_2^+(A\,^2\Pi_u, v^+ = 0-12)$ in the energy range of $17.0 - 18.2$ eV," J. Chem. Phys. **112**, 1271–1278 (2000).

[S7] J. A. Coxon and M. P. Haley, "Rotational analysis of the $A\,^2\Pi_u \rightarrow X\,^2\Pi_g$ second negative band system of $^{16}O_2^+$," J. Mol. Spec. **108**, 119–136 (1984).

[S8] John Brown and Alan Carrington, *Rotational Spectroscopy of Diatomic Molecules* (Cambridge University Press, 2003).

[S9] W. Kong and J. W. Hepburn, "PFI-ZEKE spectroscopy using coherent vacuum UV: $O_2^+(a\,^4\Pi_u) \leftarrow O_2(X\,^3\Sigma_g^-)$," Int. J. Mass Spectrom. Ion Proc. **159**, 27–35 (1996).